Optical and Quantum Electronics (2023) 55:163
https://doi.org/10.1007/s11082-022-04433-w

The influence of a trap state on the photoluminescence decay times under single pulse excitation

K. P. Chiu[1]

Received: 16 October 2022 / Accepted: 25 November 2022 / Published online: 3 January 2023

Abstract
We numerically calculated the time-resolved photoluminescence spectra using the bimolecular trapping-detrapping model. The variations of carrier lifetimes are investigated by changing the carrier recombination and trapping rate constants, as well as the concentration of available trapping states.

Keywords Time-resolved photoluminescence · Bimolecular trapping-detrapping model · Triexponential decaying function

1 Introduction

Perovskite materials are recently attracted a lot of attentions in the research area of solar cell applications. Their outstanding intrinsic properties, such as high absorption coefficient (Wolf 2014), tunable band gap (Noh et al. 2013; Snaith 2013), large carrier diffusion-length (Edri et al. 2014; Zhao et al. 2014; Dong et al. 2015; Chen et al. 2017) and carrier mobility (Stranks et al. 2013; Stoumpos et al. 2013; Ponseca et al. 2014), show the potential improvement in the photovoltaic performance of a solar cell. However, to the practical purpose in designing the optoelectronic device and improving its photovoltaic efficiency, it needs to understand the fundamental interactions between photons and the carriers in the material. Time-resolved photoluminescence (TRPL) spectroscopy is one of the powerful techniques to investigate the mechanism of electron transition processes in photoluminescence (PL) materials (Lin et al. 2017; Cai et al. 2020). In this work, we will numerically analyze and discuss the evolution of the excitonic and non-radiative trap state electron populations in the perovskite material with respect to time using the bimolecular trapping-detrapping model (Chirvony et al. 2016, 2017; Péan et al. 2020). From the results of time evolution populations, it is possible to imitate the TRPL spectra of the sample.

To the best of our knowledge, most of the researches related to the analyses of TRPL spectra usually based on known lifetimes, which are obtained from directly fitting experimentally measured TRPL spectra or from other experimental measurements, and further to

✉ K. P. Chiu
kpchiu@cycu.edu.tw

[1] Department of Physics, Chung Yuan Christian University, No. 200, Zhongbei Rd., Zhongli Dist., Taoyuan City 320314, Taiwan, R.O.C.

investigate the properties of the kinetics of carrier transitions associated with the material studied. Also, most researches related to the lifetimes of TRPL spectra usually focus on discussing the properties of the intensity- or amplitude-averaged lifetimes, which can be more properly associated with an experimentally measured lifetime. Here, we try to start from given parameters related to the kinetics of carrier transitions, and further to numerically investigate their influence on the TRPL lifetimes. The properties and variation trends of each individual lifetimes are discussed. The influence of different material parameters, such as the radiative and non-radiative carrier transition rates, the electron trapping and detrapping rate constants (Chiu 2022), and the concentration of available trap state, on the behavior of TRPL can be systematically analyzed. These results can provide helpful information to understand the connection between the physical processes happened within the material and the observed TRPL spectra.

2 Numerical calculation model

In the following calculations, we consider the phenomenological model depicted in Fig. 1. We want to imitate the properties of PL in a three-level system. There are two distinct states for electrons: the excited state with energy level slightly above but comparable to the conduction band minimum (CBM) and the non-radiative trap state with energy level below the band edge (Stranks et al. 2014; Yamada et al. 2016; Mandal et al. 2020). The photo-generated electrons in the excited state can recombine with the holes in the valance band through three different transition processes: the radiative electron–hole recombination process with transition rate constant k_R (cm^3ns^{-1}), the non-radiative electron–hole recombination process with transition rate constant k_N (cm^3ns^{-1}), and the non-radiative trapping-detrapping process through the trap state with electron trapping and detrapping rate constants k_T (cm^3ns^{-1}) and k_D (cm^3ns^{-1}), respectively. The PL light comes only from the radiative recombination of electrons in the excited state with the holes in the valance band.

The physical mechanism of the radiative electron–hole recombination is associated with the excitonic or band-to-band recombinations (Stranks et al. 2014; Yamada et al. 2016). And the mechanism of non-radiative electron–hole recombination is resulted from shallow trap state-mediated Auger recombination (Stranks et al. 2014; Péan et al. 2020). And,

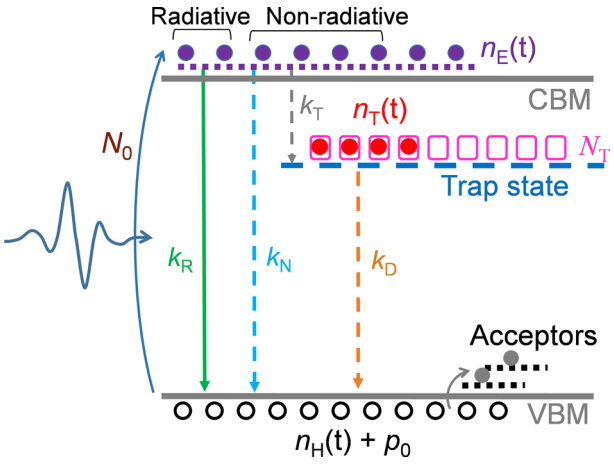

Fig. 1 Schematic diagram for describing the transition processes of the photoexcited carriers

we consider the subgap trap state, which is due to the defect or thermally activated atomic vacancies, as to provide another non-radiative charge-trapping pathways in the carrier transition process (Shkrob et al. 2014; Stranks et al. 2014; Yin et al. 2014; Talite et al. 2016; Péan et al. 2020). There is likely to be a distribution of nonradiative trap states at different subgap energies, but they are shown here at a single energy for simplicity (Stranks et al. 2014; Péan et al. 2020). For the luminescence due to excitonic or band-to-band radiative recombination, the TRPL spectrum can properly be fitted by a distributed exponential decay function with two or three decay times.

The positive doping is considered to be an impurity-induced doping which might affect the hole energy levels in the valance band or act as an acceptor (Meggiolaro et al. 2018; Sabino et al. 2022). The energy level of the acceptor is assumed to be located above the valence band maximum. Therefore, the positive doping considered here should affect mainly on the relative portion of radiative and non-radiative recombination of the electron–hole pairs. Otherwise, the doping could also affect the energy level of trap states, Fermi energy and even the energy band gap, which will in consequence affect the PL wavelength as well as the TRPL lifetime (Pavesi 1996; Huang et al. 2004; Timmerman et al. 2012; Mir et al. 2020). On the other hand, the positively doping center can also lead to the fluctuations of the local nanoenvironment, which plays a role in affecting the transition rate constants and in consequence the inverse power law behavior of the TRPL decay (Kuno et al. 2001, 2003; Peterson et al. 2009). However, since the effects of recombination energies and the environmental dependence of the transition rate constants are still not involved in our homemade calculation program. The influence of different doping concentrations on the TRPL decay is not investigated in the present work.

The total concentration of the available trap state is N_T (cm^{-3}). The concentration of photo-generated electrons produced by illuminating a single pumping pulse is N_0 (cm^{-3}). After the single pulse excitation, some of the photo-generated electrons will recombine with the holes in the valance band, and some of them will transit into the trap state. The trapped electrons then recombine with the holes in the valance band through the detrapping process. The time dependent concentrations of electrons in the excited and trap states are n_E (cm^{-3}) and n_T (cm^{-3}), respectively. And the associated time dependent concentration of photo-generated holes in the valance band is n_H (cm^{-3}). Considering the sample is positively doped with doping concentration p_0 (cm^{-3}). Therefore, the total concentration of holes in the valance band is (n_H+p_0) after the pumping pulse. In our calculations, the bimolecular trapping-detrapping model is used to describe the time rate of change of each carrier concentration. The carrier concentrations of n_E, n_H and n_T after single pulse excitation can be described by the following set of differential equations.

$$\begin{aligned} dn_E/dt &= -k_B n_E(n_H + p_0) - k_T n_E(N_T - n_T) \\ dn_H/dt &= -k_B n_E(n_H + p_0) - k_D n_T(n_H + p_0) \\ dn_T/dt &= +k_T n_E(N_T \ldots n_T) - k_D n_T(n_H + p_0) \end{aligned} \tag{1}$$

The rate constant k_B is the combination of radiative and non-radiative recombination rate constants, i.e. $k_B=(k_R+k_N)$. The electron trapping and detrapping rate constants are k_T and k_D, respectively. We use the fifth order Runge–Kutta method (Cheney and Kincaid 2008) to solve (1) with initial values $n_E(0)=n_H(0)=N_0$, $n_T(0)=0$. And the time dependent evolutions of $n_E(t)$, $n_H(t)$ and $n_T(t)$ for different values of k_B, k_D, k_T and N_T are calculated in our following studies. To investigate the influence of the power of the pumping pulse,

Fig. 2 The calculated TRPL spectra for different values of **a** $k_B = 20, 40, 60, 100, 140 \times 10^{-20} (cm^3 ns^{-1})$, **b** $k_D = 20, 40, 60, 100, 140 \times 10^{-20} (cm^3 ns^{-1})$, **c** $k_T = 200, 400, 600, 1000, 6000 \times 10^{-20} (cm^3 ns^{-1})$, and **d** $N_T = 40, 100, 200, 300, 400 \times 10^{12} (cm^{-3})$

different values of N_0 is also used in our calculations. In order to investigate the properties of TRPL spectrum corresponding to the system, the TRPL intensity is estimated by

$$I_{TRPL}(t) = k_R n_E(t)[n_H(t) + p_0)]. \quad (2)$$

The default parameters used in our calculations are $N_0 = 500 \times 10^{12}$ (cm^{-3}), $N_T = 60 \times 10^{12}$ (cm^{-3}), $p_0 = 65 \times 10^{12}$ (cm^{-3}), $k_B = 60 \times 10^{-20}$ ($cm^3 ns^{-1}$), $k_R = 0.8 k_B$, $k_D = 80 \times 10^{-20}$ ($cm^3 ns^{-1}$), and $k_T = 6000 \times 10^{-20}$ ($cm^3 ns^{-1}$). These default parameters and the variation range of the parameters used in the following calculations are mainly referred to the reference (Péan 2020) and the references in it (Hutter et al. 2015; Brenes et al. 2017).

With changing single parameter once a time, the TRPL spectra for different parameters are calculated using (2) after solving the time evolutions of the carrier concentrations from (1). And the associated luminescence lifetimes are obtained by fitting each calculated TRPL spectrum using a combination of exponentially decaying functions. Although, in a real material, the rate constants are usually as a function of excitation intensity, pulse duration, temperature of the surroundings etc. (Greben et al. 2017; Wright et al. 2017; Mandal et al. 2020; Ha et al. 2021; Chen et al. 2021) These effects are not involved in our present calculation program.

3 Results and discussion

The results shown in Fig. 2a–d are the calculated TRPL spectra using the default parameters but changing the value of k_B, k_D, k_T, and N_T, respectively. The increasing in k_B affects the TRPL spectra more obviously in the medium and long-time duration after the excitation pulse. And, the increasing in k_D and k_T mainly affect the behavior of TRPL spectra in the long-time duration and in the time duration just after the excitation pulse, respectively. The increasing in N_T seems to affect the TRPL spectra more obviously in full time duration of the calculations. To quantitatively analyze the variations of the carrier lifetimes with different parameters, the TRPL spectra are fitted by a tri-exponential decaying function $A_1 \exp(-t/\tau_1) + A_2 \exp(-t/\tau_2) + A_1 \exp(-t/\tau_3)$. In the analysis of a time-resolved PL spectrum, the most usually used fitting functions are bi-exponential and tri-exponential decay functions. In our calculated results, a bi-exponential decay function cannot well fit all the TRPL spectra we have calculated for different parameters. Therefore, we choose a tri-exponential decay function, which can well fit all the calculated spectrum results, to fit our calculated TRPL spectra to obtain the carrier lifetimes.

The variations of the fitted carrier lifetimes with increasing k_B, k_D, and k_T are shown in Fig. 3. With increasing k_B, the long lifetime (τ_3 and medium lifetime (τ_2 decrease gradually, but the short lifetime (τ_1 remains unchanged at about 35–40 ns. The increasing k_D results in slightly decreasing in τ_2 and τ_3, and has almost no effect on τ_1. With increasing k_T, all the three lifetimes rapidly decrease until k_T reaches the value about 1000×10^{-20} ($cm^3 ns^{-1}$). For even larger k_T, each lifetime changes slowly with increasing k_T. From the results shown in Fig. 3, we can see that the property of the short lifetime, τ_1, is only correlated with the trapping rate constant of the trap state. The property of the medium lifetime, τ_2, is strongly affected by both the recombination rate constant and trapping rate constant.

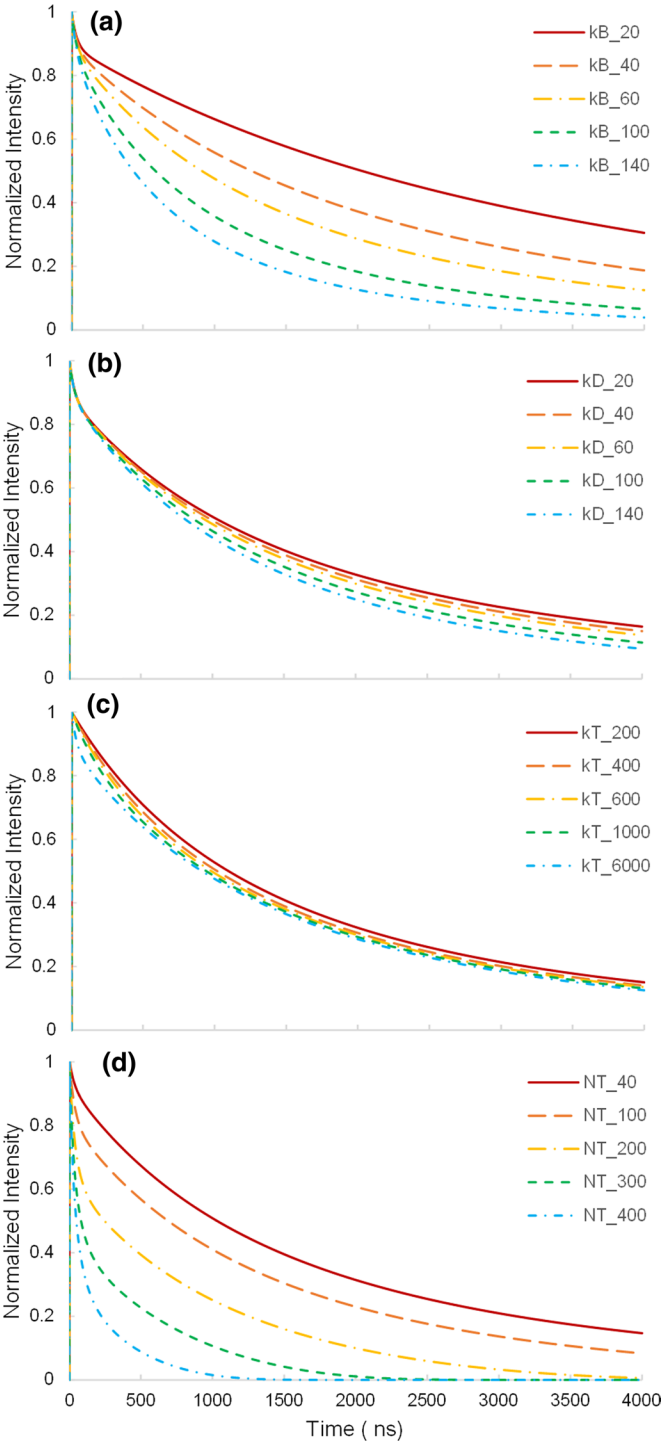
(a)
kB_20
kB_40
kB_60
kB_100
kB_140
(b)
kD_20
kD_40
kD_60
kD_100
kD_140
(c)
kT_200
kT_400
kT_600
kT_1000
kT_6000
(d)
NT_40
NT_100
NT_200
NT_300
NT_400
Normalized Intensity
0
0.2
0.4
0.6
0.8
1
0
500
1000
1500
2000
2500
3000
3500
4000
Time (ns)

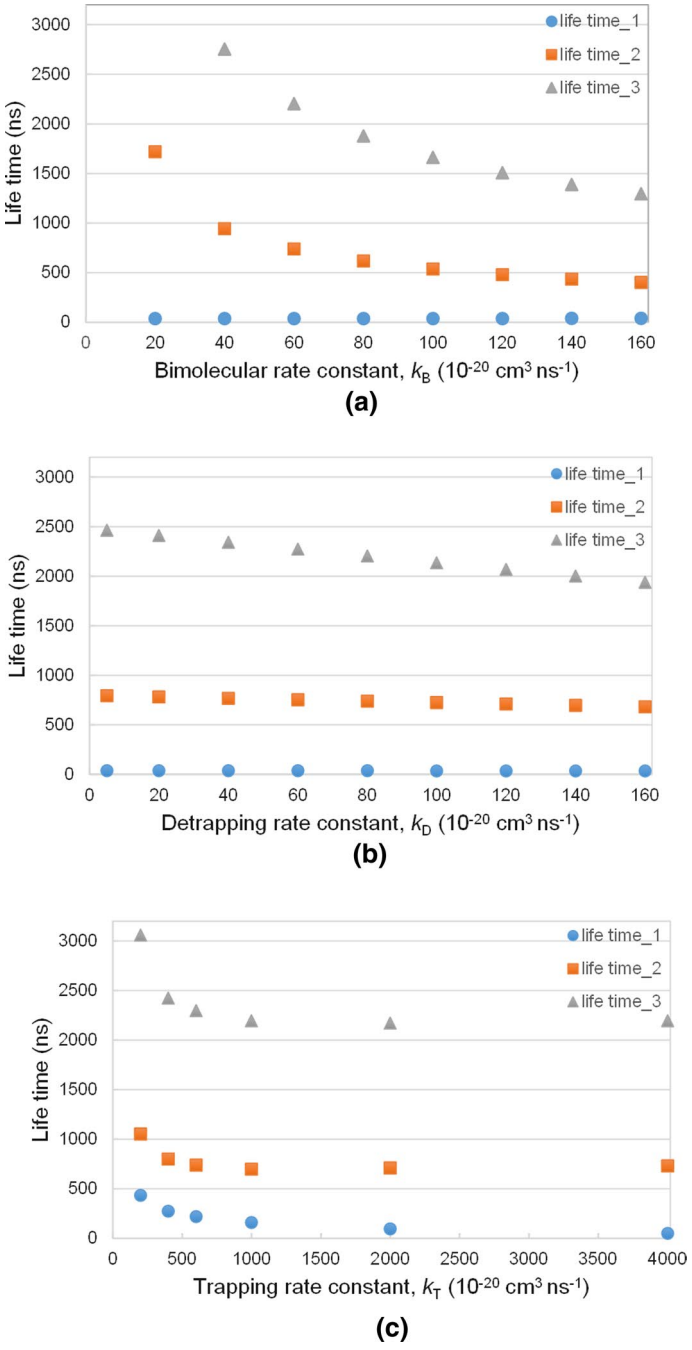

Fig. 3 The variations of fitted lifetimes from the calculated TRPL spectra using the default parameters but with **a** different k_B, **b** different k_D, and **c** different k_T

And the behavior of the long lifetime, τ_3 , dependents on each of the rate constants. Based

on these observations the lifetime τ_1 should be correlated with the recombination process that occurs when the electron concentration of the trap state, n_T, is low. In this situation, the concentration n_E decreases rapidly mainly due to the transition of electrons into the trap state and the effect of detrapping of electrons in the trap state is negligible. The intensity of luminescence is therefore decreasing rapidly, and the larger the trapping rate constant k_T the shorter the lifetime τ_1 .

On the other hand, because of increasing k_B and k_T both result in reducing the lifetime τ_2 , it should be correlated with the recombination process that occurs when n_T becomes larger but is still unsaturated. In this situation, the rate of decreasing in n_E due to the trapping effect becomes smaller and the detrapping effect of the electrons in the trap state is still obscure. Therefore, the larger k_B or k_T will leads to a smaller τ_2 , and the increase in k_D is only slightly reducing τ_2 . Finally, the lifetime τ_3 should be correlated with the recombination process when n_T approaches its saturation value and even begins to decrease from the saturation. In this situation, the increase in either k_B, k_D or k_T will increase the rate change of n_E and n_H, therefore, reducing the lifetime τ_3 . This can also explain why the τ_3 is more obviously influenced by the detrapping rate constant in this condition.

We also calculated the TRPL spectra for different concentrations of available trap state, N_T. Figure 4 shows the variations of the three fitted lifetimes when changing the value of N_T with other parameters are remained as the default values. The inset in Fig. 4 shows the results for $\tau_{1\,1}$ with a magnified vertical scale. When the available trap state is larger, more electrons in the excited state can be trapped into the trap state. This will result in a larger decreasing rate of n_E in the time period of just after the pumping pulse and till n_T reaching its saturation. Therefore, the three lifetimes of the TRPL spectra tend to decrease with increasing N_T. It is interesting to note that $\tau_{1\,1}$ and $\tau_{1\,2}$ seems to change their behavior when N_T is larger than 200×10^{12} (cm^{-3}) which is about $0.4N_0$.

To see what happened to cause this change, we demonstrate the evolutions of n_E, n_H and n_T with time for the N_T values of 100×10^{12}, 220×10^{12} and 400×10^{12} (cm^{-3}), respectively, in Fig. 5. The results in Fig. 5a represent the situation for relatively small N_T. We can see that the concentration of trapped electrons, n_T, reaches its saturation value quickly and remains at saturation for a long time. The variations of τ_1 and τ_2 with different N_T are relatively small in this situation because these two lifetimes are correlated with the recombination process that occurs when n_T is still unsaturated. The results in Fig. 5b represent the situation for relatively large N_T, that is, in the region when the lifetimes suddenly decrease with increasing N_T. The concentration n_T still can reach its saturation value in this situation, but the concentration of n_E has decreased to a value which is comparable to or smaller than the saturation value of n_T. The recombination processes associated with τ_1 and τ_2 might be seriously interrupting by the process associated with τ_3 . The results in Fig. 5c represent the situation for even larger N_T. We can see that n_T cannot reach its saturation value and n_E quickly decreases to very small values in this situation.

From the results in Figs. 3c and 4, we can see that the variation property of the lifetimes for small N_T (when k_T is fixed) behaves similar to that for large k_T (when N_T is fixed). The changes in the lifetimes are slowly in these situations. This behavior could be attributed to the concentration of trapped electron approaching to its saturation condition completely and there are still abundant photo-generated electrons after the saturation. The recombination processes associated with each lifetime in the system can be proceeded completely. On the other hand, the variation property of the lifetimes for large N_T (when k_T is fixed) behaves similar to that for small k_T (when N_T is fixed). The variations of the lifetimes with the corresponding parameter are more obvious in these situations, which could be explained by the reason described in the discussions of the results shown in Fig. 5b, c.

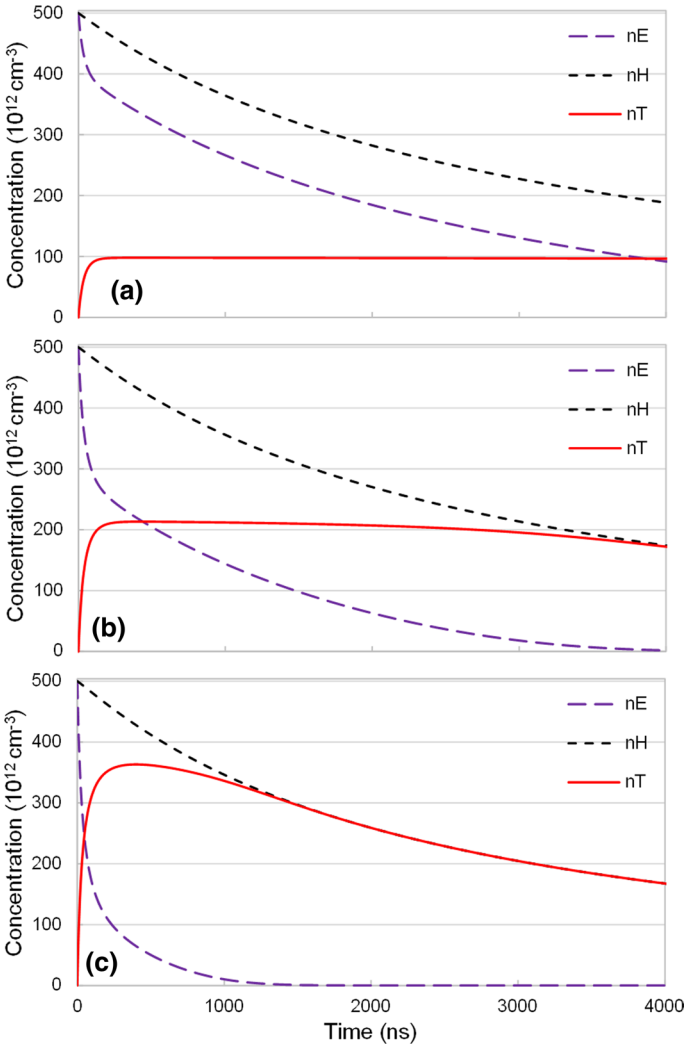

Fig. 4 The evolutions of n_E, n_H and n_T with time for different values of N_T. **a** $N_T = 100 \times 10^{12}(\text{cm}^{-3})$, **b** $N_T = 220 \times 10^{12}(\text{cm}^{-3})$ and **c** $N_T = 400 \times 10^{12}(\text{cm}^{-3})$

4 Conclusion

The properties of TRPL spectra corresponding to the carrier recombination processes with one shallow trap state mediated in the energy gap are numerically discussed in this work. The bimolecular trapping-detrapping model are used to describe the transitions of photo-generated carriers in our calculations. Time evaluations of the carrier concentrations involved in the recombination processes are solved by the fifth order Runge–Kutta method, and the TRPL spectra are calculated accordingly. The resulted TRPL spectra can be fitted by a triexponential decaying function to obtain three luminescence lifetimes. The value of the short lifetime is mainly affected by the rate constant k_T. and is

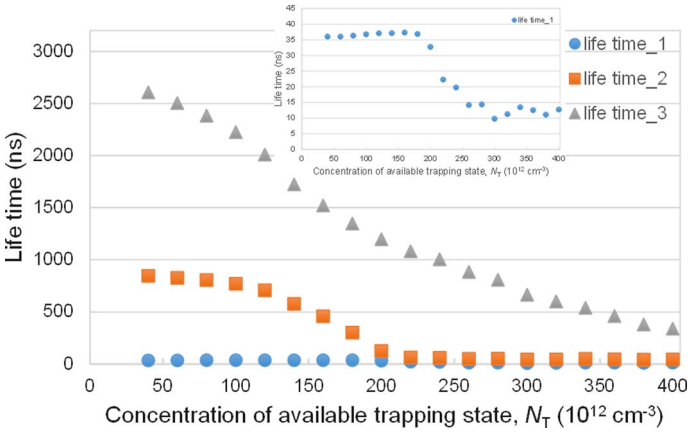

Fig. 5 The variations of fitted TRPL lifetimes with increasing N_T

almost independent of the rate constant k_D. The value of the medium lifetime is mainly affected by the rate constants k_B and k_T. These two luminescence lifetimes could be associated with the carrier recombination processes that occur under the situation when the electrons in the non-radiative trap state are still unsaturated. The value of the long lifetime is affected by either the rate constants k_B, k_D and k_T. It could be associated with the carrier recombination process that occurs when the electrons in the trap state approaches its saturation condition and even after.

Acknowledgements This work was supported by the Ministry of Science and Technology, Taiwan. Grant numbers are MOST 110-2112-M-033-012 and MOST 111-2112-M-033-008.

Authors' contributions This declaration is "not applicable". KPC wrote the main manuscript text and prepared figures.

Funding This work was supported by the Ministry of Science and Technology, Taiwan. Grant numbers are MOST 110–2112-M-033–012 and MOST 111–2112-M-033–008.

Availability of data and materials The datasets generated during and/or analyzed during the current study are available from the corresponding author on reasonable request.

Declarations

Conflict of interest The authors declare no competing interests.

Ethical approval This declaration is "not applicable".

References

Brenes, R., Guo, D., Osherov, A., Noel, N.K., Eames, C., Hutter, E.M., Pathak, S.K., Niroui, F., Friend, R.H., Islam, M.S., Snaith, H.J., Bulović, V., Savenije, T.J., Stranks, S.D.: Metal halide perovskite polycrystalline films exhibiting properties of single crystals. Joule **1**, 155–167 (2017)

Cheney, W., Kincaid, D.: Numerical mathematics and computing. In: Ordinary Differential Equations, Chapter 10, 6th edn. pp. 439–464. Thomson Brooks/Cole (2008).

Chirvony, V.S., Carrero, S.G., Suárez, I., Galian, R.E., Sessolo, M., Bolink, H.J., Pastor, J.P.M., Prieto, J.P.: Interfacial charge-carrier trapping in $CH_3NH_3PbI_3$-based heterolayered structures revealed by time-resolved photoluminescence spectroscopy. J. Phys. Chem. Lett. **7**, 1972–1977 (2016)

Chirvony, V.S., Carrero, S.G., Suárez, I., Galian, R.E., Sessolo, M., Bolink, H.J., Pastor, J.P.M., Prieto, J.P.: Delayed luminescence in lead halide perovskite nanocrystals. J. Phys. Chem. C **121**, 13381–13390 (2017)

Chen, T., Chen, W.L., Foley, B.J., Lee, J., Ruff, J.P.C., Ko, J.Y.P., Brown, C.M., Harriger, L.W., Zhang, D., Park, C., Yoon, M., Chang, Y.M., Choi, J.J., Lee, S.H.: Origin of long lifetime of band-edge charge carriers in organic–inorganic lead iodide perovskites. PANS **114**, 7519–7524 (2017)

Cai, K.B., Huang, H.Y., Chen, P.W., Wen, X.M., Li, K., Capinig, K.C., Shen, J.L., Chiu, K.P., Yuan, C.T.: Highly transparent and luminescent gel glass based on reabsorption-free gold nanoclusters. Nanoscale **12**, 10781–10789 (2020)

Chen, J., Zhang, C., Liu, X., Peng, L., Lin, J.: Chen, X: Carrier dynamic process in all-inorganic halide perovskites explored by photoluminescence spectra. Photon. Res. **9**, 151–170 (2021)

Chiu, K.P.: The variations of photoluminescence decay times under the influence of a trapping state. In: 22nd International Conference on Numerical Simulation of Optoelectronic Devices, Politecnico di Torino, Italy (2022)

Dong, Q., Fang, Y., Shao, Y., Mulligan, P., Qiu, J., Cao, L., Huang, J.: Electron-hole diffusion lengths > 175 μm in solution-grown $CH_3NH_3PbI_3$ single crystals. Science **347**, 967–970 (2015)

Edri, E., Kirmayer, S., Mukhopadhyay, S., Gartsman, K., Hodes, G., Cahen, D.: Elucidating the charge carrier separation and working mechanism of $CH_3NH_3PbI_{3-x}Cl_x$ perovskite solar cell. Nat. Commun. **5**, 3461 (2014)

Greben, M., Khoroshyy, P., Gutsch, S., Hiller, D.: Changes of the absorption cross section of Si nanocrystals with temperature and distance. Beilstein J. Nanotechnol. **8**, 2315–2323 (2017)

Huang, J.S., Luo, X.D., Yang, X.D., Sun, Z., Sun, B.Q., Xu, Z.Y., Ge, W.K.: Abnormal energy dependence of photoluminescence decay time in InGaN epilayer. Chin. Phys. Lett. **21**, 2529–2532 (2004)

Hutter, E.M., Eperon, G.E., Stranks, S.D., Savenije, T.J.: Charge carriers in planar and meso-structured organic-inorganic perovskites: mobilities, lifetimes, and concentrations of trap states. J. Phys. Chem. Lett. **6**, 3082–3090 (2015)

Ha, S.K., Wu, W.S., Powers, E.R., Paritmongkol, W., Tisdale, W.A.: Power-dependent photoluminescence efficiency in manganese-doped 2D hybrid perovskite nanoplatelets. ACS Nano **15**, 20527–20538 (2021)

Kuno, M., Fromm, D.P., Gallagher, A., Nesbitt, D.J., Micic, O.I., Nozik, A.J.: Fluorescence intermittency in single InP quantum dots. Nano Lett. **1**, 557–564 (2001)

Kuno, M., Fromm, D.P., Johnson, S.T., Gallagher, A., Nesbitt, D.J.: Modeling distributed kinetics in isolated semiconductor quantum dots. Phys. Rev. B **67**, 125304 (2003)

Lin, H.T., Cai, K.B., Huang, H.Y., Lin, T.N., Shen, J.L., Lin, C.A.J., Yuan, C.T.: Thermally-activated delayed fluorescence from biocompatible, solid-state gold nanoclusters embedded into ionic-crystal matrices. J. Lumin. **187**, 269–273 (2017)

Meggiolaro, D., Motti, S.G., Mosconi, E., Barker, A.J., Ball, J., Perini, C.A.R., Deschler, F., Petrozza, A., Angelis, F.D.: Iodine chemistry determines the defect tolerance of lead-halide perovskites. Energy Environ. Sci. **11**, 702–713 (2018)

Mandal, S., Mukherjee, S., De, C.K., Roy, D., Ghosh, S., Mandal, P.K.: Extent of shallow/deep trap states beyond the conduction band minimum in defect-tolerant CsPbBr3 perovskite quantum dot: control over the degree of charge carrier recombination. J. Phys. Chem. Lett. **11**, 1702–1707 (2020)

Mir, W.J., Sheikh, T., Arfin, H., Xia, Z., Nag, A.: Lanthanide doping in metal halide perovskite nanocrystals: spectral shifting, quantum cutting and optoelectronic applications. NPG Asia Mater. **12**, 9 (2020)

Noh, J.H., Im, S.H., Heo, J.H., Mandal, T.N., Seok, S.I.: Chemical management for colorful, efficient, and stable inorganic–organic hybrid nanostructured solar cells. Nano Lett. **13**, 1764–1769 (2013)

Pavesi, L.: Influence of dispersive exciton motion on the recombination dynamics in porous silicon. J. Appl. Phys. **80**, 216–225 (1996)

Peterson, J.J., Nesbitt, D.J.: Modified power law behavior in quantum dot blinking: a novel role for biexcitons and Auger ionization. Nano Lett. **9**, 338–345 (2009)

Ponseca, C.S., Jr., Savenije, T.J., Abdellah, M., Zheng, K., Yartsev, A., Pascher, T., Harlang, T., Chabera, P., Pullerits, T., Stepanov, A., Wolf, J.P., Sundström, V.: Organometal halide perovskite solar cell materials rationalized: ultrafast charge generation, high and microsecond-long balanced mobilities, and slow recombination. J. Am. Chem. Soc. **136**, 5189–5192 (2014)

Péan, E.V., Dimitrov, S., Castroc, C.S., Davies, M.L.: Interpreting time-resolved photoluminescence of perovskite materials. Phys. Chem. Chem. Phys. **22**, 28345–28358 (2020)

Snaith, H.J.: Perovskites: the emergence of a new era for low-cost, high-efficiency solar cells. J. Phys. Chem. Lett. **4**, 3623–3630 (2013)

Stoumpos, C.C., Malliakas, C.D., Kanatzidis, M.G.: Semiconducting tin and lead iodide perovskites with organic cations: phase transitions, high mobilities, and near-infrared photoluminescent properties. Inorg. Chem. **52**, 9019–9038 (2013)

Stranks, S.D., Eperon, G.E., Grancini, G., Menelaou, C., Alcocer, M.J.P., Leijtens, T., Herz, L.M., Petrozza, A., Snaith, H.J.: Electron-hole diffusion lengths exceeding 1 micrometer in an organometal trihalide perovskite absorber. Science **342**, 341–344 (2013)

Shkrob, I.A., Marin, T.W.: Charge trapping in photovoltaically active perovskites and related halogenoplumbate compounds. J. Phys. Chem. Lett. **5**, 1066 (2014)

Stranks, S.D., Burlakov, V.M., Leijtens, T., Ball, J.M., Goriely, A., Snaith, H.J.: Recombination kinetics in organic-inorganic perovskites: excitons, free charge, and subgap states. Phys. Rev. Appl. **2**, 034007 (2014)

Sabino, F.P., Zunger, A., Dalpian, G.M.: Intrinsic doping limitations in inorganic lead halide perovskites. Mater. Horiz. **9**, 791–803 (2022)

Timmerman, D., Gregorkiewicz, T.: Power-dependent spectral shift of photoluminescence from ensembles of silicon nanocrystals. Nanoscale Res. Lett. **7**, 389 (2012)

Talite, M.J.A., Lin, H.T., Jiang, Z.C., Lin, T.N., Huang, H.Y., Heredia, E., Flores, A., Chao, Y.C., Shen, J.L., Lin, C.A.J., Yuan, C.T.: Solid-state, ambient-operation thermally activated delayed fluorescence from flexible, non-toxic gold-nanocluster thin films: towards the development of biocompatible light-emitting devices. Nanotechnology **27**, 345701 (2016)

Wolf, S.D., Holovsky, J., Moon, S.J., Loper, P., Niesen, B., Ledinsky, M., Haug, F.J., Yum, J.H., Ballif, C.: Organometallic halide perovskites: sharp optical absorption edge and its relation to photovoltaic performance. J. Phys. Chem. Lett. **5**, 1035–1039 (2014)

Wright, A.D., Milot, R.L., Eperon, G.E., Snaith, H.J.: Band-tail recombination in hybrid lead iodide perovskite. Adv. Funct. Mater. **27**, 1700860 (2017)

Yin, W.J., Shi, T., Yan, Y.: Unusual defect physics in $CH_3NH_3PbI_3$ perovskite solar cell absorber. Appl. Phys. Lett. **104**, 063903 (2014)

Yamada, Y., Yamada, T., Shimazaki, A., Wakamiya, A., Kanemitsu, Y.: Interfacial charge-carrier trapping in $CH_3NH_3PbI_3$-based heterolayered structures revealed by time-resolved photoluminescence spectroscopy. J. Phys. Chem. Lett. **7**, 1972–1977 (2016)

Zhao, Y., Nardes, A.M., Zhu, K.: Solid-state mesostructured perovskite $CH_3NH_3PbI_3$ solar cells: charge transport, recombination, and diffusion length. J. Phys. Chem. Lett. **5**, 490–494 (2014)